Forestry An International Journal of Forest Research

Institute of Chartered Foresters

Forestry 2015; **88**, 304–316, doi:10.1093/forestry/cpu050
Advance Access publication 8 December 2014

Assessing height changes in a highly structured forest using regularly acquired aerial image data

Christoph Stepper[1]*, Christoph Straub[1] and Hans Pretzsch[2]

[1]*Department of Information Technology, Research Group: Remote Sensing, Bavarian State Institute of Forestry (LWF), Hans-Carl-von-Carlowitz-Platz 1, Freising D-85354, Germany*
[2]*Chair for Forest Growth and Yield Science, Faculty of Forest Science and Resource Management, Technische Universität München, Hans-Carl-von-Carlowitz-Platz 2, Freising D-85354, Germany*

*Corresponding author. Tel: +49 8161712609; Fax: +49 8161714971; E-mail: christoph.stepper@lwf.bayern.de

Received 31 July 2014

In this paper, we demonstrate the effectiveness of digital stereo images and canopy height models (CHMs) derived from them for forest height change assessment. Top heights were derived for 199 terrestrial inventory plots from forest inventories conducted in 2008 and 2013 in a forest near Traunstein, Germany. Semi-Global Matching was applied to two sets of aerial stereo images, acquired in 2009 and 2012, respectively, to compute CHMs. Subsequently, several height percentiles were calculated from the areas in the CHMs that lay within the inventory plot locations. The maximum CHM value (h_{max}) had the highest correlation with the field-based canopy top heights and was selected for use in all further analysis. Periodic annual increments (PAIs) of forest height were calculated from both the remote sensing and the field data at the inventory plot locations. Scatterplots of the PAIs over top height revealed similar patterns in the results derived from the two data sets. The inventory plots were assigned to three height classes representing various forest successional stages – *youth*, *full vigour* and *old age*. The PAI distributions within the three height classes were significantly different from one another. Our findings suggest that CHMs derived from repeat aerial image surveys can be a viable tool to measure canopy heights and to assess forest height changes over time, even for a highly structured, mixed forest in central Europe.

Introduction

Tree height measurements provide valuable insight into the vertical structure of forest stands (Brokaw *et al.*, 1999). In combination with measurements of diameter at breast height (DBH), tree heights are often used to estimate growing stock attributes such as timber volume. Moreover, in both forest practice and forest science, tree heights serve as indicators of site quality and are used to quantify yield (Kramer and Akça, 2008). Terrestrial measurements of tree heights within traditional forest inventories, however, are costly and very time-consuming (Næsset and Økland, 2002). Also, because these measurements of tree crown apices are done in scattered inventory plots, data only exist for small areas of the forest, and little information is available for the forest areas between the plots. Additionally, most forest inventories, at least in central Europe, are repeated only every 10 to 20 years, meaning that no new measurements are available for relatively long periods. However, as Holopainen *et al.* (2014) pointed out, precise and up-to-date information are indispensable for the implementation of sustainable forest management practices. To overcome the common shortcomings of most terrestrial inventories, i.e. the unavailability of wall-to-wall data and the long periods where no new data are available, regularly acquired data from remote sensing technologies capable of capturing the height of forest canopies could be very useful.

With the advent of LiDAR (Light Detection and Ranging), forest researchers began to use these data for forest attribute estimation. As early as 1984, Nelson *et al.* (1984) reported results for the assessment of tree heights and canopy profiles using a profiling laser system. Airborne laser scanning systems for use in forestry became popular during the 1990s. Different studies were conducted to estimate stand height and timber volume using these data – in the beginning, primarily for boreal forests (e.g. Nilsson, 1996; Næsset, 1997). LiDAR technology and forestry applications have matured rapidly and moved from the research to the operational realm (Hudak *et al.*, 2009).

A number of studies have been conducted in order to investigate LiDAR for the estimation of change. McRoberts *et al.* (2014) provided an overview of LiDAR-based change assessment studies and distinguished them into two groups – single-tree studies and area-based studies. In single-tree approaches for estimating change, mostly individual crown segments are considered and height growth is usually assessed using maximum heights within these crown segments derived from multi-temporal LiDAR data.

Such single-tree studies were published by, e.g. Hyyppä *et al.* (2003), St-Onge and Vepakomma (2004), Yu *et al.* (2004) and Yu *et al.* (2006). They concluded that estimation of forest height change is effective using multi-temporal LiDAR data. Area-based studies have focused rather more on larger areas such as forest inventory plots and, in addition to canopy height changes, have

looked at changes in aggregated forest attributes such as timber volume or biomass per unit area (McRoberts *et al.*, 2014). In most of these investigations, characteristics derived from LiDAR height distributions were used for modelling. Area-based change studies were described, e.g. by Næsset and Gobakken (2005), Yu *et al.* (2008), Hopkinson *et al.* (2008), Hudak *et al.* (2012), and Bollandsås *et al.* (2013). Despite the rather short time intervals between the repeated acquisitions dates employed in these studies, the potential of LiDAR for estimating forest growth in terms of changes in stand height, basal area or biomass was confirmed.

One drawback of LiDAR systems for monitoring forest stands, however, is the relatively high cost of data acquisition. In several European countries, surveying authorities have carried out nationwide LiDAR programs commissioned for generating digital terrain models (DTMs) with high accuracy. For example, the surveying authority in the state of Bavaria, Germany, computed a LiDAR-based DTM with 1 m resolution for the entire area of the state. However, regularly scheduled LiDAR acquisitions have, thus far, not been planned.

In contrast, in many areas, a tradition of conducting periodic aerial image surveys was established decades ago. Such surveys began, for example, in Bavaria in 1985 (Stößel, 2009) and are currently repeated at regular 3-year intervals. The development of digital aerial cameras (Leberl *et al.*, 2012) and their implementation in most administrative surveys further simplified the provision of and improved the availability of aerial imagery. The processing chain has become completely digital, and due to progress in computer technology – including new algorithms for image matching such as Semi-Global Matching (SGM; Hirschmüller, 2008) – dense height data can now be computed from such imagery (Haala, 2013).

Prior to the introduction of digital cameras for aerial surveys, analogue photographs (mainly panchromatic and colour-infrared) were the primary source data for aerial photogrammetry. For digital (softcopy) photogrammetry applications (using either stereoscopic photo interpretation at digital photogrammetric workstations or automatic image-matching procedures), the images had to be digitized before use. Some studies, carried out in the early 2000s, examined the feasibility of using digitized aerial photographs and conventional automatic image-matching algorithms (e.g. cross-correlation) to determine forest heights. Næsset (2002) and Korpela and Anttila (2004) used digitized analogue photographs to generate elevation data for forest stands in south-eastern Norway and southern Finland, respectively. In both studies, mean stand heights computed from terrestrial measurements were compared with various percentiles of the image-based height data. Zagalikis *et al.* (2005) demonstrated the potential of digitized aerial photographs in conjunction with existing terrain data for automatic height extraction of single trees in Sitka spruce plantations in Scotland.

Due to the existence of a long series of analogue photographs for different areas, some studies have utilized these data to investigate forest canopy height dynamics over decades. As examples, studies from Wales (Miller *et al.*, 2000), Japan (Itaya *et al.*, 2004) and Canada (Véga and St-Onge, 2008) have all demonstrated the applicability of historical photographs for the generation of surface models using image-matching technologies. By applying these derived surface models to forest change assessment, these authors were also able to detect vertical growth and gap dynamics in forest canopies.

However, as White *et al.* (2013b) stated, height measurements derived from image matching of aerial images describe the upper canopy surface only. Thus, to achieve heights above ground, additional bare earth elevations are necessary. LiDAR measurements have been proven to serve this purpose well, and assuming that the terrain surface under a forest remains approximately constant over time, existing LiDAR-based DTMs from topographic mapping surveys can be utilized for height normalization of image-based measurements.

Thus, St-Onge and Achaichia (2001) and St-Onge *et al.* (2004) evaluated the combination of LiDAR and digital photogrammetry as a mapping tool for quantifying forest structural characteristics and individual tree heights. St-Onge and Achaichia (2001) analysed two CHMs, one using LiDAR only and one using image-based surface heights normalized against LiDAR ground elevations. They found that the pattern determined by the variation of stand height and density were similar from each other. The image-based CHM was capable to resolve tree clusters and even the crowns of single trees. Photogrammetric measurements of individual tree apex heights in combination with LiDAR ground elevations were used to estimate individual tree heights. Using field-measured tree heights for evaluation resulted in an average bias of 0.59 m (St-Onge *et al.*, 2004). In a rigorous comparison of heights from image-based CHMs and reference LiDAR-only CHMs, it was shown that high correlations, both at the pixel level (correlation coefficient up to 0.89) and at the plot level (correlation coefficient up to 0.95), were achievable (St-Onge *et al.*, 2008b). Characteristics describing the vertical distribution of the forest canopy surface were largely similar between the two data sets. Thus, the authors concluded that aerial images from recurrent surveys in conjunction with existing LiDAR-based DTMs might be a viable data combination for monitoring changes in forest structure over time.

As a possible approach for mire ecosystem monitoring, Waser *et al.* (2008) presented a workflow for the assessment of forest area change by means of image-based CHMs, computed from the combination of digitized aerial images acquired 5 years apart and national LiDAR data of Switzerland. Moreover, Baltsavias *et al.* (2008) demonstrated the great potential of repeat aerial imagery for forest growth assessment. In this study, dense image matching was applied to two sets of digitized aerial images acquired 5 years apart for a test site in western Switzerland. Individual tree heights were extracted from the image-based CHMs, and growth rates were calculated for the 5-year period between the acquisition dates of the two images. Their results encourage further investigation.

As stated above, recent developments in image-matching algorithms and the extensive availability of digital aerial imagery have stimulated the use of image-based height information for forestry applications. Example studies were conducted for the detection of single trees (Hirschmugl *et al.*, 2007), the assessment of forest canopy heights (Wallerman *et al.*, 2012) and the modelling of various forest attributes, e.g. basal area and timber volume (Bohlin *et al.*, 2012; Järnstedt *et al.*, 2012; Nurminen *et al.*, 2013; Straub *et al.*, 2013a; Vastaranta *et al.*, 2013; Rahlf *et al.*, 2014; Stepper *et al.*, 2015). Thus, photogrammetry is experiencing a renaissance in forest research at the moment. However, up to now, little work has been done to investigate the efficacy of repeat aerial surveys, providing high-resolution digital images, for use in forest height change assessment, particularly for complex forests in central Europe. Due to the possibilities for computing dense measurements of the canopy surface, this tool might prove quite

effective for acquiring information about the complex dynamics of forest height structure.

Thus, our primary objective with this study was to scrutinize the use of digital aerial imagery from regularly repeated surveys for assessing forest height changes at the plot level for a complex, highly structured forest in southern Germany. The specific tasks undertaken in this study were as follows:

- Application of SGM to automatically compute image-based canopy height models (CHMs) for two image data sets acquired as part of the regularly scheduled aerial image surveys already taking place in Bavaria.
- Derivation and comparison of the periodic annual increments (PAI) of forest height computed from the two CHMs and two corresponding field inventory data sets at geo-referenced forest inventory plots.
- Analysis of the PAIs in height for three height classes representing different successional stages – *youth*, *full vigour* and *old age*.

Materials

Test site

The study is centred on the *Traunstein* test site, a highly structured forest near the city of Traunstein in Bavaria, Germany. This forest has been used as test site for several remote-sensing studies, e.g. Mette (2007), Schneider *et al.* (2012), Straub *et al.* (2013a) and Straub *et al.* (2013b). The geographic location of the test site (~240 ha; latitude: 47° 52′ N, longitude: 12° 38′ E) is shown in the inset of Figure 1. Elevations range from 575 to 695 m above sea level, and the topography is best described as a variation of flat and undulating terrain interspersed with steeply cut valleys (cf. main illustration in Figure 1). The commonly occurring soils are predominantly made up of glacial sediments, and the climate is characterized by a mean annual temperature of 7.3° Celsius and a mean annual precipitation of 1600 mm, with high amounts of rainfall in summer. Thereby, good site conditions for forest growth prevail within the *Traunstein* test site, and stand productivity is within the upper third of the central European range (Moshammer and Pretzsch, 2010). Field measurements from two consecutive forest inventories carried out in 2008 and 2013 (a description of the field data will follow in the next section) were available, and as shown in Table 1, the principal tree species are Norway spruce (*Picea abies* [L.] Karst.), European beech (*Fagus sylvatica* L.) and white fir (*Abies alba* Mill.).

Major storm events, which occurred in 2007 (*Kyrill*) and 2008 (*Paula* and *Emma*), affected primarily mature spruce stands at the site. The subsequent regeneration in the wind-throw areas is now dominated by broadleaf trees. The test-site forest stands

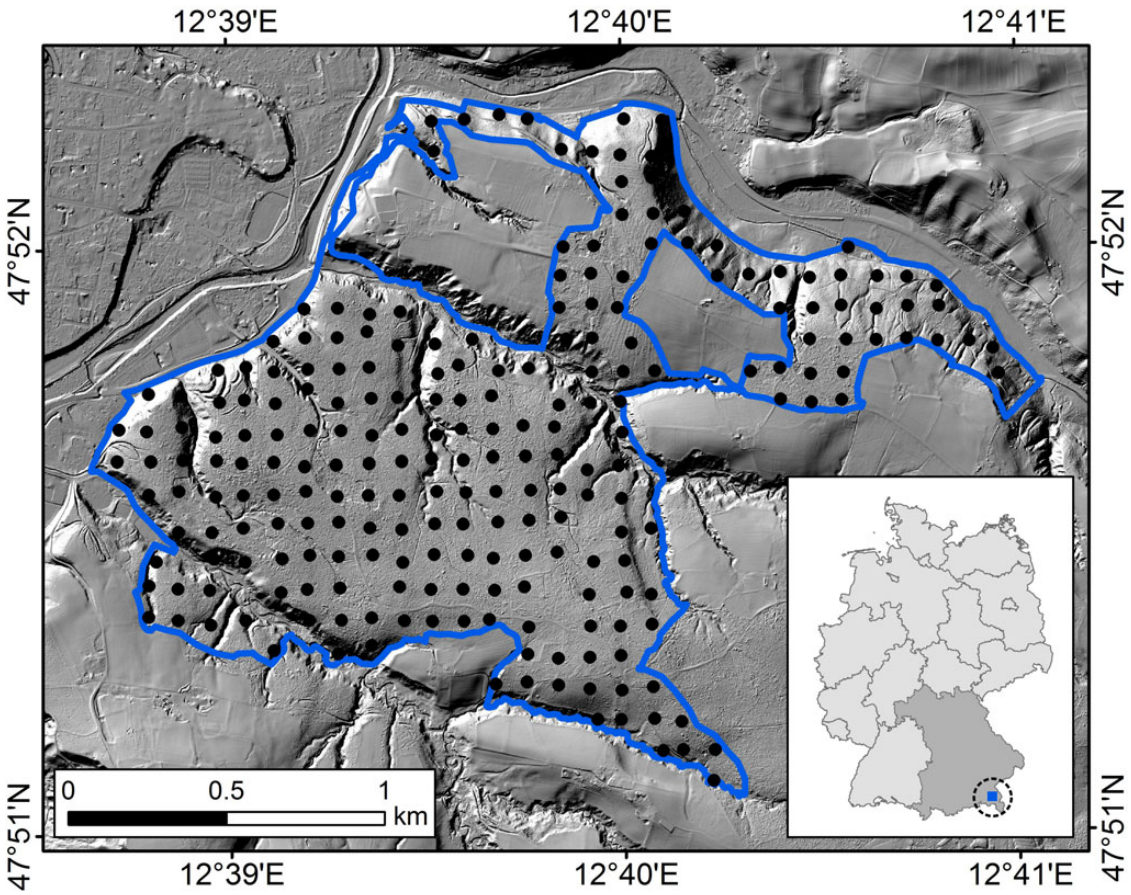

Figure 1 Geographic location of the *Traunstein* test site in south-eastern Bavaria, Germany. The inset map displays the location of the test site in Germany (light grey) and that in Bavaria (dark grey), respectively. The main illustration shows the outer boundary of the test site and the spatial distribution of the forest inventory plots, superimposed on a relief image derived from a LiDAR-DTM.

Table 1 Tree species composition in the *Traunstein* test site (given as percentage of the basal area) calculated using field inventory data collected in 2008 and 2013

Species	2008	2013
Norway spruce (%)	43	39
White fir (%)	14	16
European beech (%)	22	24
Others (%)	21	21

The table shows that the proportion of spruce decreased by 4 per cent between the two inventories, whereas both the beech and fir proportions increased by 2 per cent.

are part of the municipal forest which belongs to the city of Traunstein and are actively managed to support an uneven-aged mixed-species forest with the dominant tree species being spruce, beech and fir. In summary, the forest within the *Traunstein* test site comprises a great variety of successional stages, i.e. heterogeneous species composition, many different age classes and multi-layered stands. Thus, the test site is well suited for the investigation of forest canopy height changes, due to both the presence of good site conditions for forest growth and the broad range of successional stages with highly variable canopy heights.

Field measurements

Field measurements were made available to us from two terrestrial inventories that were carried out in August 2008 and July–November 2013 by staff from the Chair for Forest Growth and Yield Science at the Technische Universität München. The field plots where the data were collected – 228, in total, within the test site – are laid out in a regular grid pattern of 100 m × 100 m, each meant to represent roughly 1 ha of forested land (cf. Figure 1). The plot centres are permanently marked, and during the inventories, a Trimble Pathfinder ProXT global positioning system (GPS) unit combined with an external Hurricane L1 antenna was used to record the centre point of every inventory plot. Generally, the GPS measurements achieved accuracies with maximum deviations of ±3 m (R. Moshammer, personal communication, 9 October 2014).

Within each sample plot, all relevant tree attributes (e.g. tree species, DBH and age class) were recorded for all trees within one of three concentric circles based on thresholds of DBH. These concentric circles and the trees recorded within them are defined by the following radii r_i and corresponding DBH thresholds (in parenthesis): 3.15 m (DBH $<$ 10 cm), 6.31 m (10 $\leq$ DBH $<$ 30 cm) and 12.62 m (DBH $\geq$ 30 cm). On average (standard deviation in parenthesis), 14.3 (6.2) trees and 14.9 (7.6) trees were callipered at each plot in 2008 and 2013, respectively. The area of the largest circle, where all trees greater than 30 cm DBH were recorded, is 500 m^2. This particular area was used as the reference region for the linkage to the remotely sensed data in the study. For a more general description of the concentric sampling method used, refer to van Laar and Akça (2007).

In addition to the above-mentioned attributes, tree heights were recorded for several representative trees at each of the inventory plots. All trees were assigned to one of the following vertical layers: regeneration, understory, overstory or emergent trees (i.e. trees with crowns that emerge above the rest of the canopy). For every existing combination of tree species, age class and vertical layer affiliation occurring at a plot, at least one tree height was measured. If available, the height of at least two trees per present combination at each plot was measured for each of the following species: Norway spruce (*P. abies* [L.] Karst.), Scots pine (*Pinus sylvestris* L.), white fir (*A. alba* Mill.), European larch (*Larix decidua* Mill.), Douglas fir (*Pseudotsuga menziesii* [Mirb.] Franco), European beech (*F. sylvatica* L.) and English/sessile oak (*Quercus robur* L./*Quercus petrea* [Matt.] Liebl.). Trees with broken treetops were preferably not selected for height measurement. Thus, depending on the vertical structure, density and tree species mixture of the forest, the number of height measurements ranged from 1 to 30 (average: 9.1, standard deviation: 4.7) per plot in 2008 and from 2 to 25 (average: 8.1, standard deviation: 3.7) in 2013. Tree heights were measured by means of a Vertex IV hypsometer (Haglöf Sweden, 2007) using ultrasonic distance measuring and electronic clinometer techniques. Based on the measured distance to the tree trunk and the angle to the apex, the heights were calculated trigonometrically. According to the manufacturer's statement, measurement errors were not expected to exceed 1%. The height of each treetop was measured three times from the same vantage point, and the average was recorded as the tree height. Based on the measured tree heights and DBHs, generalized height-diameter functions (describing diameter–height relationships) were adjusted to the respective conditions at each plot. By this means, tree heights could be modelled for all remaining trees in the plots for which no terrestrial height measurement was recorded. Thus, field-measured inventory data, in particular, tree height data, were available for the years 2008 and 2013.

Aerial image data

All remote sensing data used in our study were provided by the Bavarian Surveying Administration. The aerial imagery was acquired in the years 2009 and 2012 as part of the regularly scheduled aerial survey of Bavaria, which is updated every three years (Stößel, 2009). The 2009 survey was conducted on 25 April 2009 using an UltraCam X camera (Vexcel Imaging GmbH, a Microsoft Company, Graz, Austria) with forward and side overlaps of 65 and 30%, respectively, whereas the 2012 survey was conducted on 16 June 2012 with an UltraCam Eagle camera with forward and side overlaps of 75 and 35%, respectively (Figure 2). The flights were carried out at survey altitudes of 2370 m (2009) and 2830 m (2012) above mean ground level to achieve a ground sampling distance (GSD) of 0.20 m. The data were provided to us as panchromatic images (PAN, 12-bit radiometric resolution), in conjunction with the respective camera protocols including the interior orientation parameters (pixel size, focal length and principal point). Additionally, we received the results from the aerial triangulations, i.e. the exterior orientation parameters defining the position and angular orientation of the images (sensor position: x, y, z; rotation angles: roll ω, pitch ϕ, yaw κ). According to the vendor, the image orientation of the 2012 survey was validated with twelve independent ground control points. The RMS accuracy of the orientation was 14.4, 21.2 and 7.9 cm in the X, Y and Z directions, respectively. We assume similar accuracies for the 2009 survey, as no independent accuracy assessment of the image orientation was conducted for this data set.

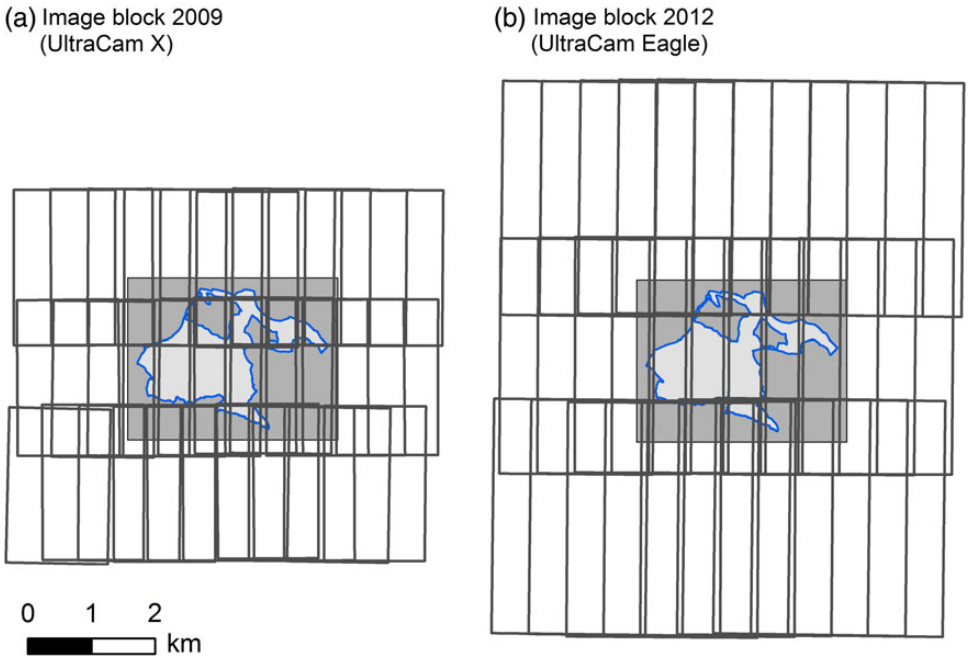

Figure 2 Image blocks of the digital stereo images from the aerial surveys conducted in 2009 (a) and 2012 (b) for the *Traunstein* test site. The dark-grey boxes in both subfigures indicate the map extent displayed in Figure 1, and the light-grey areas show the extent of the test site.

Table 2 Acquisition parameters of the 2009 and 2012 aerial image surveys

	2009	2012
Camera	UltraCam X	UltraCam Eagle
Date of flight	25 April 2009	16 June 2012
GSD (m)	0.20	0.20
No. of images	30	27
No. of flight lines	3	3
Forward overlap	65%	75%
Side overlap	30%	35%

The characteristics of the two flights are summarized in Table 2, and image blocks displaying the overlapping stereo images covering the test site are shown in Figure 2. The dark-grey boxes indicate the map extent displayed in Figure 1, and the light-grey areas show the extent of the actual test site.

As height data obtained from image matching of the aerial stereo images reflect the canopy surface in metres above sea level, additional bare earth information is necessary in order to compute canopy heights above ground. For this purpose, we used a LiDAR-based DTM (1 m spatial resolution) derived from the official topographic mapping survey in 2010 with a last return density of 5–6 measurements per square metre (LVG, 2012).

Methods

An overview of the methodological workflow is diagrammed in Figure 3.

Image matching and derivation of CHMs

Image matching was conducted for the two image blocks acquired from the regular aerial surveys done in 2009 and 2012. For this purpose, we applied the Semi-Global Matching (SGM) approach to compute a very dense coverage of height measurements in the area covered by the respective image blocks. The core algorithm of SGM, as developed by Hirschmüller (2008), aggregates pixel-wise matching costs calculated along 1D paths at every 45° from a given starting point, i.e. the base image pixel location. Matching costs measure the dissimilarity between corresponding pixels in two images – the base and match image – and by penalizing disparity jumps with additional costs, smooth disparities along the search path are ensured (Hirschmüller, 2011). The minimum aggregated costs for each base image pixel are used to create the disparity map for each stereo pair and, after performing forward intersections, the resulting height measurements are obtained (Gehrke *et al.*, 2010). Thus, the pixel-wise SGM is capable of computing dense height measurements with reasonable processing runtime on large images (Haala, 2011).

In this study, we used the Remote Sensing Software Package Graz (RSG, version 7.44, see Joanneum Research, 2014) to accomplish image matching with the SGM method. Due to the relatively small side overlap of the stereo images (cf. Figure 2), only along track stereo image pairs were considered for computation. In total, 27 stereo image pairs from 2009 and 24 stereo image pairs from 2012 were processed. Within RSG, dense image matching was executed separately for each stereo pair. The pixel-wise measurements at a GSD-resolution of 0.20 m were aggregated to 1 m pixels, assigning the elevation of the highest measurement to the respective grid cell centre. Subsequently, the single stereo image pairs were merged by means of a probabilistic range image fusion approach (Rumpler *et al.*, 2013). Eventually, two digital surface models (DSM, 1 m resolution) were created – one for each of the two image blocks (i.e. 2009 and 2012). Finally, CHMs were derived by subtracting the elevation values of the bare earth DTM from the *z*-values of the two DSMs.

As mentioned, e.g. by Hopkinson *et al.* (2008), both vertical accuracy and consistency between height measurements collected at two different

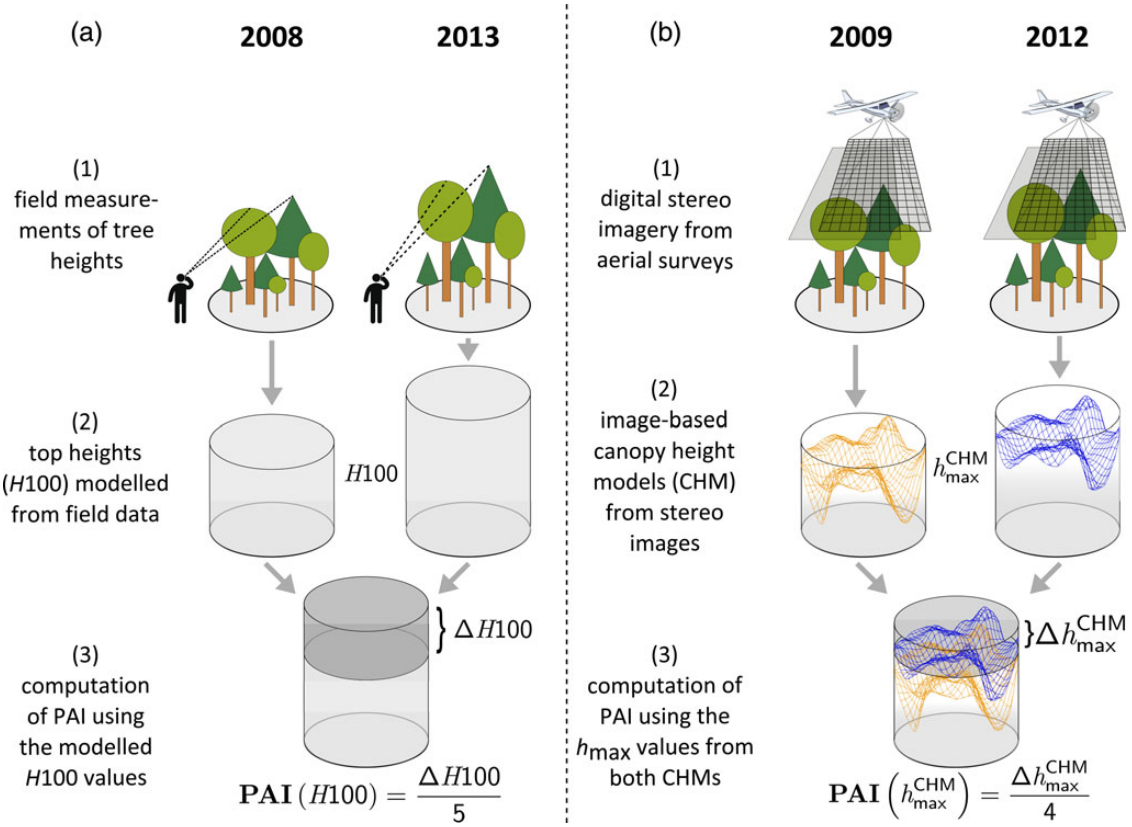

Figure 3 Methodological workflow used to conduct a height change assessment with changes quantified in terms of PAI. (a) Terrestrial assessment: (1) tree crown heights were measured for representative samples at the respective inventory plots, (2) top heights (*H*100) were modelled using the height measurements of trees from the overstory and emergent tree layers, (3) PAI was calculated as the difference between the modelled *H*100 values for the two inventory dates divided by the number of shoot elongation periods (which in this case is equal to the number of years between the two inventories). (b) Aerial image assessment: (1) digital stereo images were acquired in regularly scheduled aerial surveys, (2) CHMs were created by subtracting LiDAR-derived terrain heights from image-based surface models, (3) PAI was computed as the difference between the maximum height values (h_{max}) from the two CHMs divided by the number of shoot elongation periods between the two image dates (in this case, not equal to the number of years between the images due to seasonal differences between the two acquisition dates).

times are crucial to the success of change detection applications, as any small but systematic error might result in a false assessment of change. This is especially important in the case of data with short time intervals between acquisition dates, as were used in our study. To ensure that no systematic elevation shift existed between the two CHMs, the heights calculated from each of the two image data sets for six sports fields (i.e. relatively large areas with very homogenous heights) near the forest area under investigation were compared. The mean shift in height found for these control surfaces was −0.12 m (SD: 0.25 m) when the CHM-heights from 2009 were subtracted from those derived from the 2012 image data. We considered this to be a marginal shift attributable to random errors in the data and, therefore, judged the CHMs to be adequately accurate for forest height change assessment. Thus, using the two derived CHMs, various height percentiles (25th, 50th, 75th, 90th, 95th and maximum) describing the vertical structure of the canopy surface were calculated for the area within each of the 500 m^2 circular inventory plots.

Identification of suitable inventory plots for height change assessment

Prior to making any further calculations, it was necessary to examine the suitability of the field plots for height change assessment. Three different criteria were used to identify possible outliers among the plots: (1) substantial harvesting that took place between the date of the field inventory and the corresponding aerial survey, (2) edge effects (i.e. tree crowns located along the plot boundary were included in the measurements of the CHMs, but the corresponding stem position was actually outside of the plot. Therefore, these tree data were not included in the field measurements; see White *et al.*, 2013a), and (3) gross errors from the matching process. In this study, we specified gross matching errors as one or two neighbouring pixels of the CHM, which were considerably higher (threshold >15 m) than the surrounding pixels within the area of an inventory plot. Based on visual examination of the two CHMs and corresponding colour-infra-red orthoimages, we identified 11, 8 and 10 plots for substantial harvesting, edge effects and gross matching errors, respectively. Thus, in total, 29 plots were eliminated from the data set prior to further processing, resulting in 199 inventory plots that remained for the height change assessment. Example plots for each of the three different criteria are given in Supplementary data, Figure S1.

Computation of field-based top heights at the plot level

Image-based height measurements primarily characterize the outer envelope of the forest canopy (White *et al.*, 2013b). According to the forest mensuration textbook of van Laar and Akça (2007), aerial stereo images are

Algorithm 1 Computation of the field-based top height (*H*100), defined as the average height of the 100 stems per hectare with the largest DBHs

```
1   Select the number of plots within the test site, n
2   for i = 1 to n do
3     Select all measured trees assigned to either the overstory or the
      emergent tree layer, m
4     for j = 1 to m do
5       Replicate j by the representation factor RF_j and append to list L
6     end
7     Sort all items in L in descending order according to DBH
8     Select the first 100 entries of L_sort
9     Calculate arithmetic mean of the selection (H100)
10  end
```

Table 3 Descriptive statistics for the field-based top heights (*H*100) calculated from field data recorded in 2008 and 2013

	Min (m)	Median (m)	Mean (m)	Max (m)	SD (m)
2008	1.5	30.4	27.7	41.2	9.6
2013	3.0	31.4	28.8	42.2	8.8

Statistics were computed based on all 199 inventory plots in the *Traunstein* test site, which were deemed suitable for the height change assessment in this study (see the section 'Identification of suitable inventory plots for height change assessment').

suitable for measuring the top height of forest stands. Thus, we selected this height characteristic for our height change assessment. The top height (*H*100) used in this study was defined as the average height of the 100 stems per hectare with the largest DBHs. *H*100 was computed for each inventory plot as follows (cf. Algorithm 1): first, all trees assigned to either the overstory or the emergent tree layer were selected. Second, the selected tree items (including height and DBH) were replicated by their respective representation factor RF_j of the concentric sampling ($RF_j = 10\,000/(\pi \cdot r_j^2)$, with r_j is the radius of the corresponding circle). Third, the resulting item list was sorted in descending order according to DBH, and finally, the arithmetic mean of the tree heights (measured or modelled) was calculated from the first 100 entries. As a result, modelled top heights (*H*100) were available for all field plots from both the 2008 and the 2013 inventories.

Descriptive statistics of the field-based top heights (*H*100) for the years 2008 and 2013 are given in Table 3. The average plot-level top height from the 199 remaining inventory plots was 27.7 m in 2008 and 28.8 m in 2013. The high standard deviations hint at the great variability in canopy heights.

Correlation of height percentiles with field-based top heights

As has been shown in various other studies dealing with LiDAR or image-based height data (e.g. St-Onge *et al.*, 2008a; Straub *et al.*, 2009; Wasser *et al.*, 2013), upper percentile heights are typically highly correlated with field-measured canopy heights. To select the height percentile that best describes field-based top height (*H*100), we correlated the height percentiles to the field-based top heights from 2008 and 2013 (scatterplot matrices showing the pair-wise correlations between the field-based top height *H*100 and the different percentile metrics are given in Supplementary data, Figure S2). As the data were not normally distributed, we used Spearman's rank correlations to analyse the relationships between the field-based *H*100 values and the CHM-height percentiles at the corresponding inventory plots. We compared the 2009/2008 and 2012/2013 data sets separately.

Table 4 Spearman's rank correlation coefficients between plot-level CHM percentiles and the modelled *H*100 top height values (*P*-values were < 0.01 for all correlations)

Data set	hp 25	hp 50	hp 75	hp 90	hp 95	h_{max}
2009/2008	0.51	0.63	0.77	0.83	0.86	0.91
2012/2013	0.41	0.55	0.72	0.85	0.87	0.90

All 199 inventory plots in the *Traunstein* test site which were deemed suitable for the height change assessment were used (see the section 'Identification of suitable inventory plots for height change assessment').

The results of the correlation analysis between the field-based top height *H*100 and the height percentiles calculated from the CHMs are presented in Table 4. The upper percentiles from the CHM (90th, 95th and maximum) yielded correlation coefficients consistently higher than 0.80. In general, the highest correlations were observed for the maximum height of the CHM (h_{max}). The relationship between h_{max} and *H*100 is illustrated in the scatterplot in Figure 4. Overall, most points over the entire range of canopy heights are close to the 1 : 1 line, i.e. no considerable scatter is visible. This confirms that the variable h_{max} derived from the image-based CHMs is a suitable predictor for the plot-level top height in the *Traunstein* test site. Thus, the variable h_{max} was selected for the height change assessment in this study.

Height change assessment at the plot level

Height changes between the two time points were assessed both from the field measurements and the remotely sensed data. The procedure applied in this study for the calculation of periodic annual increments (PAIs) of forest height for the data sets is illustrated in Figure 3. The PAI derived from the field data (equation 1) was calculated separately for each plot by taking the difference between the modelled *H*100 values for the two inventory dates and dividing it by the number of shoot elongation periods (here equal to the number of years between the two surveys).

$$\mathrm{PAI}(H100) = \frac{H100(2013) - H100(2008)}{5} \quad (1)$$

As displayed in Table 2, the aerial images used here to compute the CHMs were acquired in different seasons. In accordance with, e.g. Hopkinson *et al.* (2008), the fact that shoot elongation is an intermittent rather than a continual process during the vegetation period must be considered with regard to height growth assessments. Lyr *et al.* (1992) found that Norway spruce, European beech and white fir – the tree species dominating the stocking in the *Traunstein* test site – follow the *Quercus*-type, meaning that height growth stops quite early in the growing season. To take the different acquisition times into account for our study, we employed phenological observations (occurrence of flushing) from a nearby level II plot of the *ICP Forests* (International Co-operative Programme on Assessment and Monitoring of Air Pollution Effects on Forests; Beuker *et al.*, 2010). At this plot, which is dominated by spruce, the growth of new needles became visible in 2009 in the time period from 28 April to 09 June. In 2012, this phenomenon was first visible in the time period between 17 April and 22 May (S. Raspe, personal communication, 8 July 2014). Based on this information, we assumed that the first aerial image acquisition (25 April 2009) was carried out before the period of rapid tree height growth in 2009, and the second acquisition (16 June 2012) was carried out after the 2012 period of rapid tree height growth.

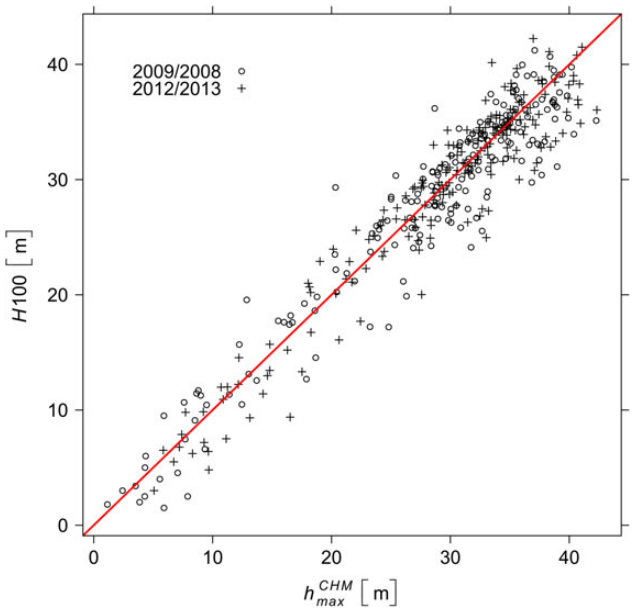

Figure 4 Scatterplot of plot-level h_{max} values extracted from the CHMs for the years 2009 and 2012 plotted against *H*100 – the top heights derived from the field measurements taken in 2008 and 2013. The scatterplot shows all 199 inventory plots in the *Traunstein* test site, which were deemed suitable for the height change assessment in this study (see the section 'Identification of suitable inventory plots for height change assessment').

Thus, with regard to the image-based canopy heights, the PAI was computed by taking the difference between the maximum height values (h_{max}) from the two CHMs and dividing it by the number of shoot elongation periods (here, this number was not equal to the number of years between the two image data sets due to different acquisition dates during the year, and their relationship to the maximum height growth periods; equation 2).

$$\mathrm{PAI}(h_{max}^{CHM}) = \frac{h_{max}^{CHM}(2012) - h_{max}^{CHM}(2009)}{4} \quad (2)$$

Scatterplots were used to analyse the relationship between initial forest height and height growth. Therefore, the PAI values obtained from the field measurements and the image-based height data were plotted against the *H*100 values computed from the 2008 field inventory data. In addition, a linear regression line was fitted to the data using least-squares adjustment.

Comparison of PAI for the different height classes

The guideline for the silvicultural treatment of spruce-dominated forest stands (Böhm, 2009; Bavarian State Forest Enterprise) provides different height thresholds for the top height of forest stands to distinguish among successional stages. Using this reference, we defined the following height classes based on the 2008 top heights to quantify different growth rates depending on initial tree height: *youth*: $H100 < 12$ m, *full vigour*: $12\ \mathrm{m} \leq H100 < 25$ m, and *old age*: $H100 \geq 25$ m. Each of the inventory plots was assigned to one of these classes, and the respective growth rates derived from the image-based CHMs were examined. A non-parametric Kruskal–Wallis rank sum test was performed to test for statistical differences between the subsets, as the normality assumption for ordinary ANOVA was not fulfilled. *Post hoc* analysis was conducted using the Wilcoxon rank sum test.

Results

Estimation of forest height change at the plot level

The overall PAI of forest height was found to be 0.22 m (SD: 0.32 m) for the field-based data, according to equation (1). Using the CHM-based measurements, the PAI was computed to be 0.30 m (SD: 0.53 m) following equation (2). Figure 5 shows scatterplots of the PAI for each inventory plot *vs* the *H*100 (2008) top heights for both the terrestrial and the aerial image-based assessment. Visual comparison of the scatterplots and the linear regression lines fitted to the data reveal similar patterns, i.e. in both cases, the height growth rates decreased with increasing *H*100. For inventory plots with a *H*100 above 25 m, the height growth was only marginally above zero. The negative growth rates found for some of the inventory plots can be explained by the fact that some single trees were removed at these plots during harvesting operations in the time period between 2008 and 2013. In general, the PAIs calculated from the image-based CHMs were somewhat higher than those derived from the field data, especially for plots with low *H*100 (2008).

Quantification of growth rates for the individual height classes

Descriptive statistics of the PAI values for the height classes *youth*, *full vigour* and *old age* (as defined in section 'Comparison of periodic annual increments for the different height classes') are presented in Table 5. Due to the great variability of obtained PAIs, the standard deviations were high for all classes. For the cohorts *youth* and *full vigour*, the standard deviations were lower than the average PAI; however, this was not the case for the class *old age*.

Figure 6 shows boxplots of the PAI values derived from the aerial image assessment, plotted separately for each of the three height classes. As could be expected based on forest growth theory (e.g. Assmann, 1970), the visual examination reveals obvious differences in the PAI among the three height classes, with a decrease in PAIs across the sequence from *youth* to *full vigour* to *old age*. To confirm this initial visual impression, a Kruskal–Wallis test was applied which revealed significant differences between the three height change distributions (P-value < 0.01). A subsequent *post hoc* analysis using the pair-wise Wilcoxon rank sum test showed that all pairs of height classes were significantly different from one another, resulting in P-values consistently below 0.01. Moreover, the boxplots for the three height classes show that the inventory plots assigned to the *youth* height class had greater variability in PAIs than those from both the *full vigour* and the *old age* height classes. Although the *old age* height class comprises the largest number of observations (about six times more than the other classes), the interquartile range of PAI values was still rather narrow. Some outliers, both in the positive and negative range, are visible and are most likely due to harvesting operations in the time period between 2008 and 2013. Additionally, some negative PAI values, predominantly occurring in the *old age* cohort, might be due to the loss of leading shoots because of wind or snow damage.

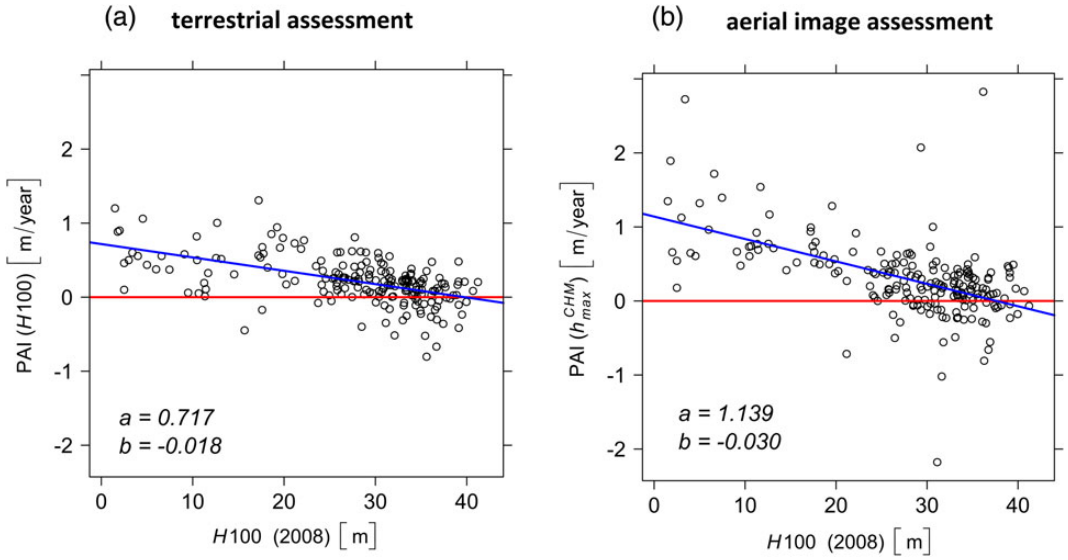

Figure 5 *H*100 (2008) top heights *vs* PAI values for the 199 inventory plots. The coefficients (*a: intercept* and *b: slope*) of the linear regression fits (trend lines) are given for both the terrestrial assessment (a) and the aerial image assessment (b).

Table 5 Descriptive statistics of the PAI values for three different height classes *youth* ($H100 < 12$ m), *full vigour* ($12\ m \leq H100 < 25$ m) and *old age* ($H100 \geq 25$ m)

Class	Min (m)	Median (m)	Mean (m)	Max (m)	SD (m)	*N*
Youth	0.18	0.76	1.01	2.73	0.58	22
Full vigour	−0.72	0.52	0.53	1.28	0.39	30
Old age	−2.18	0.16	0.15	2.83	0.45	147

N corresponds to the number of inventory plots assigned to each height class.

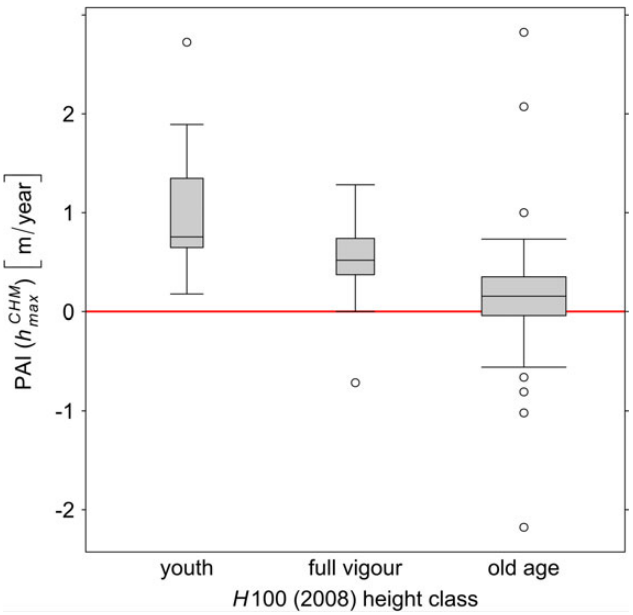

Figure 6 Boxplots of the PAI values derived from the aerial image assessment, plotted separately for each of the three height classes *youth* ($H100 < 12$ m), *full vigour* ($12\ m \leq H100 < 25$ m) and *old age* ($H100 \geq 25$ m). The width of the boxes indicates the relative number of inventory plots within each height class.

Discussion

Assessment of forest top heights using regularly acquired digital aerial imagery

The digital aerial image data used in this study were acquired as part of the regularly scheduled aerial survey undertaken by the surveying authority of the state of Bavaria, Germany. Thus, the imagery was intended for different purposes and was not primarily acquired for use in forestry applications. The two data sets used in this study were recorded with different camera types, different image overlaps and in different seasons. However, due to the fact that the basic characteristics of all images acquired as part of the regular aerial survey of Bavaria are similar (e.g. the geometric, spectral and radiometric resolutions), the images are very attractive for monitoring purposes and change assessment studies. Moreover, remote sensing approaches to vegetation structure analysis have greatly benefited from the introduction of digital cameras in aerial surveying. Compared with analogue cameras, digital cameras are able to provide panchromatic images plus multispectral information of four bands (blue, green, red and near infra-red) and have improved radiometric properties that allow for better information extraction and surface model generation.

Despite the above-mentioned differences in the data sets, detailed surface height models were successfully derived using SGM, and in combination with an additional LiDAR-based DTM, high-resolution canopy heights above ground were calculated. Very dense height measurements of the canopy surface were obtained for both data sets. High correlations with top heights from field measurements were achieved for both aerial image data sets, i.e. comparing the 2009 and 2012 CHM-heights to the

field-based top heights of 2008 and 2013, respectively (cf. Table 4). Thus, we conclude that dense matching of stereo aerial images with SGM in combination with a pre-existing LiDAR-based DTM is a viable tool for forest canopy height extraction. However, it should be considered that it was necessary to exclude 29 inventory plots for the correlation analysis because of edge effects and gross matching errors, and due to harvesting activities that occurred between the acquisition dates of the aerial imagery and the respective field surveys. With respect to applications for larger test sites, gross matching errors could be possibly eliminated automatically by using a median filter (e.g. 3×3 moving window). However, edge effects and harvesting activities have to be detected manually. In our study, the maximum height variable extracted from the CHMs had the strongest correlation to the field-based top heights. This is in line with the findings of St-Onge *et al.* (2008a) and Hopkinson *et al.* (2008) who found that higher percentiles usually have the strongest correlations with ground-measured forest heights. Additionally, in Straub *et al.* (2009), the upper percentiles derived from a LiDAR-based CHM were best correlated with the top height recorded in terrestrial inventories at the plot level when investigating a mixed forest in southern Germany.

Repeat aerial image surveys as valuable data sources for forest height change assessment

The results of our study demonstrate the feasibility of height growth detection at the plot level in complex, temperate forests based on data derived from regularly repeated aerial image surveys. Forest height change was estimated at the plot level by means of digital stereo images recorded only four growing seasons apart. Despite the relatively short time interval between the two image acquisitions, it was possible to determine reasonable PAIs. As shown in Figure 5, comparable increments with similar patterns were derived from both the terrestrial and the aerial image assessments. The difference in PAIs, especially for plots with low field-based top heights, may be attributed, at least in part, to the short time interval between the image acquisitions. We suppose that the calculated PAIs of this short period may be more affected by annual variations of growth, compared with averaging over longer time periods. In our investigation of the forest height growth increments for different top height classes that were assumed to indicate various successional stages, the highest growth rates were measured for stands in the *youth* class. The height increments derived decreased with increasing stand heights, and statistically significant differences between the increments of the respective groups were found (average PAI values for *youth*, *full vigour* and *old age*: 1.01, 0.53 and 0.15 m).

Assmann (1970) emphasized that height growth is influenced by a number of factors. Among others, these include particular characteristics of each tree species, i.e. light-demanding and shade-bearing species show different growth curves, and the effects of site, meaning that on better sites the culmination of the growth increment occurs earlier in the life of a tree than it does on poorer sites. Considering these factors, the PAIs resulting from our aerial image assessment are reasonable in view of the annual increases in height reported in the textbook by Assmann (1970). He presented the following characteristic maximum height increments for a test site from Hinterberg in the Salzkammergut, Austria: Norway spruce: 0.58 m at age 20, European beech: 0.41 m at age 23, white fir: 0.40 m at age 33. The *Traunstein* test site has good site conditions for forest growth. Thus, the higher values for tree growth we found for the *youth* class appear reasonable.

With respect to the transferability of the method presented here for height growth assessments of forests in other ecozones and with different forest management practices, the following factors should be considered: multi-species temperate forests such as the *Traunstein* forest typically achieve stand heights of 30–40 m at a stand age of 100 years. This translates to a mean annual growth rate of 0.30–0.40 m per year, or up to twice that of the growth rate of most boreal forests. Consequently, when using aerial imagery recorded within very short time intervals for image-based height change assessment – e.g. four growing seasons as in our study – measurement errors may potentially exceed growth rates. However, for fast-growing plantations – e.g. in the subtropics and tropics – even shorter intervals may be able to yield reliable information on height dynamics.

Height change as an indicator of site productivity and ecosystem diversity

Stand height and height growth over age has long been used as an indicator of site productivity (Skovsgaard and Vanclay, 2008). As stand height is rather independent from stand density (e.g. Assmann, 1970), it can be used even in managed stands as an indicator of site quality and potential productivity. However, as height is relatively expensive to measure via field surveys, and as LiDAR data are usually not acquired recurrently, the presented method for the assessment of canopy heights and height changes using digital aerial imagery has great potential for providing information about the state and the dynamics of forests. By comparing data from different time periods, shifts in stand productivity and even long trends in forest dynamics might become detectable.

Because of known allometric relationships between different stand variables such as stand height and volume (Enquist *et al.*, 2009; West *et al.*, 2009), height growth can be used as an indicator of the site-specific potential volume growth in fully stocked stands. Comparisons between this potential and the observed volume growth derived from terrestrial measurements may better reveal the effects of thinning and other disturbances on productivity, carbon sequestration and carbon stock in forest stands.

Beyond the detection of stand productivity, stand height and height dynamics, analyses such as ours may be useful in efforts to quantify and monitor ecosystem diversity as well (Noss, 1990). Habitat diversity in forests is largely influenced by the vertical stand structure, e.g. the foliage height diversity, the canopy complexity and the canopy surface roughness, and its dynamics (Lefsky *et al.*, 2002; Vierling *et al.*, 2008; Müller *et al.*, 2012; Müller and Vierling, 2014). Although the image-based height measurements can only describe the outer envelope and give no insights into the bottom to top structure within forest stands, repeated measurements of stand height using CHMs computed from aerial images can provide detailed information about changes of the canopy surface in space and time. Thus, the approach presented here may be a viable means of supporting the monitoring of structural stand dynamics caused by tree growth, silviculture and other disturbances (Hobi and Ginzler, 2012). Eventually, this might contribute to monitoring the development of habitats supplied by forested ecosystems.

Conclusion

Our study objective was to scrutinize the use of digital aerial imagery from repeat surveys for assessing forest height changes. We used aerial imagery acquired in 2009 and 2012 and field measurements recorded in 2008 and 2013 as reference data. CHMs for a highly structured forest in central Europe were computed from the two remote sensing data sets by means of Semi-Global Matching. Using the field data, field-based top heights were calculated for all inventory plots for the years 2008 and 2013.

PAIs, computed based on both the field and the remote sensing data, were then compared. The respective scatterplots of PAIs over top height revealed similar patterns. The inventory plots were assigned to three height classes representing three forest successional stages. The PAI distributions from these height classes were significantly different from one another. Thus, the results of our study are encouraging and show that repeat aerial image data can be used successfully for monitoring forest height changes over time. As the data are recorded in regular time intervals, this approach seems to be very promising for future tasks.

Future research will address the applicability of repeat aerial image surveys and automatically derived height data for modelling other changes in forest ecosystems, e.g. biomass. Moreover, we will attempt to assess single-tree height growth over time by means of image-based CHMs.

Supplementary data

Supplementary data are available at *Forestry* online.

Acknowledgements

The authors thank Stefan Kraft from the Bavarian Surveying Administration for providing the remote sensing data used in this study. They express their gratitude to Karl-Heinz Gutjahr from Joanneum Research, Graz, for his software support and to Laura Carlson for language editing. Finally, we thank Rudolf Seitz, Peter Biber and the reviewers for their helpful comments on earlier drafts of the manuscript.

Conflict of interest statement

None declared.

Funding

This work was supported by the Bavarian State Mininstry of Food, Agriculture and Forestry (in German: Bayerisches Staatsministerium für Ernährung, Landwirtschaft und Forsten).

References

Assmann, E. 1970 *The Principles of Forest Yield Study: Studies in the Organic Production, Structure, Increment and Yield of Forest Stands*. Pergamon Press, 506 p.

Baltsavias, E., Gruen, A., Eisenbeiss, H., Zhang, L. and Waser, L.T. 2008 High-quality image matching and automated generation of 3D tree models. *Int. J. Remote Sens.* **29**, 1243–1259.

Beuker, E., Raspe, S., Bastrup-Birk, A. and Preuhsler, T. 2010 Phenological observations. Manual part VI. In *ICP Forests Manual on Methods and Criteria for Harmonized Sampling, Assessment, Monitoring and Analysis of the Effects of Air Pollution on Forests: International Co-operative Programme on Assessment and Monitoring of Air Pollution Effects on Forests (ICP Forests)*. Fischer, R., Lorenz, M., Ferretti, M., Granke, O., Mues, V. and König, N. (eds). Johann Heinrich von Thünen Inst., Inst. for World Forestry.

Bohlin, J., Wallerman, J. and Fransson, J.E.S. 2012 Forest variable estimation using photogrammetric matching of digital aerial images in combination with a high-resolution DEM. *Scan. J. For. Res.* **27**, 692–699.

Böhm, H. 2009 *Waldbauhandbuch Bayerische Staatsforsten: Bewirtschaftung von Fichten- und Fichtenmischbeständen*. Stabilität – Strukturreichtum – Klimaanpassung.

Bollandsås, O.M., Gregoire, T.G., Næsset, E. and Øyen, B.-H. 2013 Detection of biomass change in a Norwegian mountain forest area using small footprint airborne laser scanner data. *Stat. Methods Appl.* **22**, 113–129.

Brokaw, N.V.L., Lent, R.A. and Hunter, M.L. 1999 Vertical structure. In *Maintaining Biodiversity in Forest Ecosystems*. Hunter, M.L. (ed). Cambridge University Press, pp. 373–399.

Enquist, B.J., West, G.B. and Brown, J.H. 2009 Extensions and evaluations of a general quantitative theory of forest structure and dynamics. *Proc. Natl Acad. Sci. USA* **106**, 7046–7051.

Gehrke, S., Morin, K., Downey, M., Boehrer, N. and Fuchs, T. 2010 Semi-global matching: an alternative to LIDAR for DSM generation? In *Proceedings of the 2010 Canadian Geomatics Conference and Symposium of Commission I: ISPRS Convergence in Geomatics – Shaping Canada's Competitive Landscape*. 15–18 June 2010, Calgary, Canada. http://www.isprs.org/proceedings/xxxviii/part1/11/11_01_Paper_121.pdf (accessed on 27 November 2014).

Haala, N. 2011 Multiray photogrammetry and dense image matching. In *Proceedings of the 53rd Photogrammetric Week*. 05–09 September 2013, Stuttgart, Germany. Fritsch, D. (ed). Wichmann Verlag, pp. 185–195.

Haala, N. 2013 The landscape of dense image matching algorithms. In *Proceedings of the 54th Photogrammetric Week*. 09–13 September 2013, Stuttgart, Germany. Fritsch, D. (ed). Wichmann Verlag, pp. 271–284.

Haglöf Sweden, A.B.. 2007 Users Guide Vertex IV and Transponder T3. http://www.haglofcg.com/index.php?option=com_docman&task=doc_view&gid=1&Itemid=100 (accessed on 09 October, 2014).

Hirschmugl, M., Ofner, M., Raggam, J. and Schardt, M. 2007 Single tree detection in very high resolution remote sensing data. *Remote Sens. Environ.* **110**, 533–544.

Hirschmüller, H. 2008 Stereo processing by Semiglobal matching and mutual information. *IEEE Trans. Pattern Anal. Mach. Intell.* **30**, 328–341.

Hirschmüller, H. 2011 Semi-global matching – motivation, developments and applications. In *Proceedings of the 53rd Photogrammetric Week*. Fritsch, D. (ed), pp. 5–11.

Hobi, M.L. and Ginzler, C. 2012 Accuracy assessment of digital surface models based on WorldView-2 and ADS80 stereo remote sensing data. *Sensors* **12**, 6347–6368.

Holopainen, M., Vastaranta, M. and Hyyppä, J. 2014 Outlook for the next generation's precision forestry in Finland. *Forests* **5**, 1682–1694.

Hopkinson, C., Chasmer, L. and Hall, R. 2008 The uncertainty in conifer plantation growth prediction from multi-temporal lidar datasets. *Remote Sens. Environ.* **112**, 1168–1180.

Hudak, A.T., Evans, J.S. and Stuart Smith, A.M. 2009 LiDAR utility for natural resource managers. *Remote Sensing* **1**, 934–951.

Hudak, A.T., Strand, E.K., Vierling, L.A., Byrne, J.C., Eitel, J.U., Martinuzzi, S. and Falkowski, M.J. 2012 Quantifying aboveground forest carbon pools and fluxes from repeat LiDAR surveys. *Remote Sens. Environ.* **123**, 25–40.

Hyyppä, J., Xiaowei, Y., Rönnholm, P. and Kaartinen, H. 2003 Factors affecting object-oriented forest growth estimates obtained using laser scanning. *Photogramm. J. Finland* **18**, 16–31.

Itaya, A., Miura, M. and Yamamoto, S.-I. 2004 Canopy height changes of an old-growth evergreen broad-leaved forest analyzed with digital elevation models. *For. Ecol. Manag.* **194**, 403–411.

Järnstedt, J., Pekkarinen, A., Tuominen, S., Ginzler, C., Holopainen, M. and Viitala, R. 2012 Forest variable estimation using a high-resolution digital surface model. *ISPRS J. Photogramm. Remote Sens.* **74**, 78–84.

Joanneum Research. 2014 Remote Sensing Software Package Graz. http://dib.joanneum.at/rsg/ (accessed on 14 February, 2014).

Korpela, I. and Anttila, P. 2004 Appraisal of the mean height of trees by means of image matching of digitised aerial photographs. *Photogramm. J. Finland* **19**, 23–36.

Kramer, H. and Akça, A. 2008 *Leitfaden zur Waldmesslehre*. 5th edn. Sauerländer, J D, x, 226 S.

Leberl, F., Gruber, M., Ponticelli, M. and Wiechert, A. 2012 The ultracam story. *Int. Arch. Photogramm. Remote Sens. Spatial Inf. Sci.* **XXXIX**, 39–44.

Lefsky, M.A., Cohen, W.B., Parker, G.G. and Harding, D.J. 2002 Lidar remote sensing for ecosystem studies. *BioScience* **52**, 19.

LVG. 2012 *Digitale Geländemodelle (DGM): Product Information of the Bavarian Office for Surveying and Geoinformation. Landesamt für Vermessung und Geoinformation Bayern*.

Lyr, H., Fiedler, H.-J. and Tranquilini, W. (eds). 1992 *Physiologie und Ökologie der Gehölze: Mit 85 Tabellen*. Fischer, 620 S.

McRoberts, R.E., Bollandsås, O.M. and Næsset, E. 2014 Modeling and estimating change. In *Forestry Applications of Airborne Laser Scanning*. Maltamo, M., Næsset, E. and Vauhkonen, J. (eds). Springer, pp. 293–313.

Mette, T. 2007 Forest biomass estimation from Polarimetric SAR Interferometry. Dissertation, DLR, Bibliotheks-und Informationswesen.

Miller, D.R., Quine, C.P. and Hadley, W. 2000 An investigation of the potential of digital photogrammetry to provide measurements of forest characteristics and abiotic damage. *For. Ecol. Manag.* **135**, 279–288.

Moshammer, R. and Pretzsch, H. 2010 *Forstwirtschaftsplan 2010: Forstbetrieb Stadtwald Traunstein*. Textteil.

Müller, J. and Vierling, K. 2014 Assessing biodiversity by airborne laser scanning. In *Forestry Applications of Airborne Laser Scanning*. Maltamo, M., Næsset, E. and Vauhkonen, J. (eds). Springer, pp. 357–374.

Müller, J., Mehr, M., Bässler, C., Fenton, M.B., Hothorn, T., Pretzsch, H. *et al*. 2012 Aggregative response in bats: prey abundance versus habitat. *Oecologia* **169**, 673–684.

Næsset, E. 1997 Determination of mean tree height of forest stands using airborne laser scanner data. *ISPRS J. Photogramm. Remote Sens.* **52**, 49–56.

Næsset, E. 2002 Determination of mean tree height of forest stands by digital photogrammetry. *Scan. J. For. Res.* **17**, 446–459.

Næsset, E. and Gobakken, T. 2005 Estimating forest growth using canopy metrics derived from airborne laser scanner data. *Remote Sens. Environ.* **96**, 453–465.

Næsset, E. and Økland, T. 2002 Estimating tree height and tree crown properties using airborne scanning laser in a boreal nature reserve. *Remote Sens. Environ.* **79**, 105–115.

Nelson, R., Krabill, W. and MacLean, G. 1984 Determining forest canopy characteristics using airborne laser data. *Remote Sens. Environ.* **15**, 201–212.

Nilsson, M. 1996 Estimation of tree heights and stand volume using an airborne lidar system. *Remote Sens. Environ.* **56**, 1–7.

Noss, R.F. 1990 Indicators for monitoring biodiversity: a hierarchical approach. *Conserv. Biol.* **4**, 355–364.

Nurminen, K., Karjalainen, M., Yu, X., Hyyppä, J. and Honkavaara, E. 2013 Performance of dense digital surface models based on image matching in the estimation of plot-level forest variables. *ISPRS J. Photogramm. Remote Sens.* **83**, 104–115.

Rahlf, J., Breidenbach, J., Solberg, S., Næsset, E. and Astrup, R. 2014 Comparison of four types of 3D data for timber volume estimation. *Remote Sens. Environ.* **155**, 325–333.

Rumpler, M., Wendel, A. and Bischof, H. 2013 Probabilistic range image integration for DSM and true-orthophoto generation. In *Image Analysis*. Kämäräinen, J.-K. and Koskela, M. (eds). Springer, pp. 533–544.

Schneider, T., Tian, J., Elatawneh, A., Rappl, A. and Reinartz, P. 2012 Tracing structural changes of a complex forest by a multiple systems approach. In *Proceedings of 1st European Association of Remote Sensing Laboratories Workshop on Temporal Analysis of Satellite Images*. EARSeL, Mykonos, Greece, pp. 159–165.

Skovsgaard, J.P. and Vanclay, J.K. 2008 Forest site productivity: a review of the evolution of dendrometric concepts for even-aged stands. *Forestry* **81**, 13–31.

Stepper, C., Straub, C. and Pretzsch, H. 2015 Using semi-global matching point clouds to estimate growing stock at the plot and stand levels: application for a broadleaf-dominated forest in central Europe. *Can. J. For. Res.* **45**, 111–123.

St-Onge, B. and Achaichia, N. 2001 Measuring forest canopy height using a combination of lidar and aerial photography data. *Int. Arch. Photogramm. Remote Sens. Spatial Inf. Sci.* **34**, 131–137.

St-Onge, B. and Vepakomma, U. 2004 Assessing forest gap dynamics and growth using multi-temporal laser-scanner data. *Power* **140**, 173–178.

St-Onge, B., Jumelet, J., Cobello, M. and Véga, C. 2004 Measuring individual tree height using a combination of stereophotogrammetry and lidar. *Can. J. For. Res.* **34**, 2122–2130.

St-Onge, B., Hu, Y. and Vega, C. 2008a Mapping the height and above-ground biomass of a mixed forest using lidar and stereo Ikonos images. *Int. J. Remote Sens.* **29**, 1277–1294.

St-Onge, B., Vega, C., Fournier, R.A. and Hu, Y. 2008b Mapping canopy height using a combination of digital stereo-photogrammetry and lidar. *Int. J. Remote Sens.* **29**, 3343–3364.

Stößel, W. 2009 Die Bayernbefliegung wird digital. *Mitteilungen des DVW e.V. Gesellschaft für Geodäsie, Geoinformation und Landmanagement*, 69–84. http://www.dvw-bayern.de/modules.php?name=wirueberuns&pa=showpage&pid=247.

Straub, C., Dees, M., Weinacker, H. and Koch, B. 2009 Using airborne laser scanner data and CIR orthophotos to estimate the stem volume of forest stands. *Photogramm. Fernerkund. Geoinf.* **2009**, 277–287.

Straub, C., Stepper, C., Seitz, R. and Waser, L.T. 2013a Potential of UltraCamX stereo images for estimating timber volume and basal area at the plot level in mixed European forests. *Can. J. For. Res.* **43**, 731–741.

Straub, C., Tian, J., Seitz, R. and Reinartz, P. 2013b Assessment of Cartosat-1 and WorldView-2 stereo imagery in combination with a LiDAR-DTM for timber volume estimation in a highly structured forest in Germany. *Forestry* **86**, 463–473.

van Laar, A. and Akça, A. 2007 *Forest Mensuration*. 2nd edn. Springer, xvi, 383.

Vastaranta, M., Wulder, M.A., White, J.C., Pekkarinen, A., Tuominen, S., Ginzler, C. *et al*. 2013 Airborne laser scanning and digital stereo imagery measures of forest structure: comparative results and implications to forest mapping and inventory update. *Can. J. Remote Sens.* **39**, 382–395.

Véga, C. and St-Onge, B. 2008 Height growth reconstruction of a boreal forest canopy over a period of 58 years using a combination of photogrammetric and lidar models. *Remote Sens. Environ.* **112**, 1784–1794.

Vierling, K.T., Vierling, L.A., Gould, W.A., Martinuzzi, S. and Clawges, R.M. 2008 Lidar: shedding new light on habitat characterization and modeling. *Front. Ecol. Environ.* **6**, 90–98.

Wallerman, J., Bohlin, J. and Fransson, J.E.S. 2012 Forest height estimation using semi-individual tree detection in multi-spectral 3D aerial DMC data. In *International Geoscience and Remote Sensing Symposium (IGARSS)*. IEEE (ed). IEEE, pp. 6372–6375.

Waser, L., Baltsavias, E., Ecker, K., Eisenbeiss, H., Feldmeyer-Christe, E., Ginzler, C. *et al*. 2008 Assessing changes of forest area and shrub encroachment in a mire ecosystem using digital surface models and CIR aerial images. *Remote Sens. Environ.* **112**, 1956–1968.

Wasser, L., Day, R., Chasmer, L., Taylor, A. and Schumann, G.J.-P. 2013 Influence of vegetation structure on lidar-derived canopy height and fractional cover in forested riparian buffers during leaf-off and leaf-on conditions. *PLoS ONE* **8**, e54776.

West, G.B., Enquist, B.J. and Brown, J.H. 2009 A general quantitative theory of forest structure and dynamics. *Proc. Natl Acad. Sci. USA* **106**, 7040–7045.

White, J.C., Wulder, M.A., Varhola, A., Vastaranta, M., Coops, N.C., Cook, B.D., Pitt, D. and Woods, M. 2013 *A best practices guide for generating forest inventory attributes from airborne laser scanning data using the area-based approach*. Information Report FI-X-10. Natural Resources Canada, Canadian Forest Service, Canadian Wood Fibre Centre, Pacific Forestry Centre, Victoria, BC, 50 p. http://cfs.nrcan.gc.ca/pubwarehouse/pdfs/34887.pdf (accessed on 27 November 2014).

White, J.C., Wulder, M.A., Vastaranta, M., Coops, N.C., Pitt, D. and Woods, M. 2013b The utility of image-based point clouds for forest inventory: a comparison with airborne laser scanning. *Forests* **4**, 518–536.

Yu, X., Hyyppä, J., Kaartinen, H. and Maltamo, M. 2004 Automatic detection of harvested trees and determination of forest growth using airborne laser scanning. *Remote Sens. Environ.* **90**, 451–462.

Yu, X., Hyyppa, J., Kukko, A., Maltamo, M. and Kaartinen, H. 2006 Change detection techniques for canopy height growth measurements using airborne laser scanner data. *Photogramm. Eng. Remote Sens.* **72**, 1339–1348.

Yu, X., Hyyppä, J., Kaartinen, H., Maltamo, M. and Hyyppä, H. 2008 Obtaining plotwise mean height and volume growth in boreal forests using multi-temporal laser surveys and various change detection techniques. *Int. J. Remote Sens.* **29**, 1367–1386.

Zagalikis, G., Cameron, A.D. and Miller, D.R. 2005 The application of digital photogrammetry and image analysis techniques to derive tree and stand characteristics. *Can. J. For. Res.* **35**, 1224–1237.